Full paper

Trimetallic Pt–Pd–Ni octahedral nanocages with subnanometer thick-wall towards high oxygen reduction reaction

Fanpeng Kong[a,b,1], Sihang Liu[c,1], Junjie Li[b], Lei Du[a], Mohammad Norouzi Banis[b], Lei Zhang[b], Guangyu Chen[a], Kieran Doyle-Davis[b], Jianneng Liang[b], Sizhe Wang[b], Feipeng Zhao[b], Ruying Li[b], Chunyu Du[a], Geping Yin[a,**], Zhijian Zhao[c,***], Xueliang Sun[b,*]

[a] State Key Laboratory of Urban Water Resource and Environment, School of Chemistry and Chemical Engineering, Harbin Institute of Technology, 150001, China
[b] Department of Mechanical and Materials Engineering, University of Western Ontario, London, ON N6A 5B9, Canada
[c] Key Laboratory for Green Chemical Technology of Ministry of Education, School of Chemical Engineering and Technology, Tianjin University, 300072, China

A B S T R A C T

Precisely engineering the composition and structure of nanomaterials can effectively tune their activity and stability towards oxygen reduction reaction (ORR), a key process in fuel cells. Here, a highly active and stable electrocatalyst for ORR is fabricated by alloying Ni atoms with octahedral Pt–Pd nanocages with ultrathin walls and exposed (111) facets. The specific activity ($3.8\ mA/cm^2$) and mass activity ($1.17\ A/mg_{Pt}$) of the octahedral Pt–Pd–Ni nanocages represent a performance enhancement by a factor of 25 and 10 compared to commercial Pt/C, respectively. In addition, the ORR activity of octahedral Pt–Pd–Ni nanocages significantly outperforms the octahedral Pt–Pd nanocages ($1.89\ mA/cm^2$ and $0.73\ A/mg_{Pt}$ in specific and mass activity). The ligand effect and compressive strain, confirmed by the X-ray absorption fine structure (XAFS) analysis and density functional theory (DFT) calculations, accounts for the enhanced activity by weakening the adsorption energy of hydroxyl groups. Particularly, it shows robust stability with only 16% decay in the mass activity after accelerating degradation tests (ADTs), rationalized by its structural stability and high vacancy formation energy. This work provides a new class of Pt based nanocatalysts with high activity and stability for ORR.

1. Introduction

Hydrogen, as a renewable and green energy carrier, has triggered extensive attention because its large-scale deployment potentially lowers not only the emission of greenhouse gases and other pollutants but also the dependence on traditional fossil fuels in the long-term [1]. Proton exchange membrane fuel cells (PEMFCs) that can effectively convert clean hydrogen and air into electricity are a promising energy conversion device for transportation [2,3]. However, the widespread application of PEMFCs is significantly hindered by its high cost, because the cathodic ORR is highly sluggish and consequently requires a large amount of Pt to accelerate the ORR kinetics [4]. Accordingly, improving the mass activity of Pt nanocatalysts towards ORR is of great concern for minimizing the cost and enabling the commercialization of PEMFCs [5,6].

During the past decades, massive efforts have been initiated to improve the mass activity of Pt-based catalysts towards ORR by improving the utilization efficiency of Pt atoms and modifying the geometric and electronic structure of surface Pt atoms [7–9]. Reducing the size of Pt-based nanoparticles is a conventional solution to increase the proportion of exposed Pt atoms on the surface and thus reduce the total Pt loading [10]. However, nanoscale particles show a lack of stability as the particles aggregate via Ostwald ripening, and fail to optimize Pt activity [11]. Impressively, core-shell structures (PtM@Pt, PdM@Pt, M = Fe, Co and Ni), synthesized by under potential deposition or dealloying [12–16], offer a rational model structure with not only high Pt utilization efficiency but also well-tuned intrinsic activity by substrates. Pt₃Ni (111) with a segregated Pt surface and Ni-rich subsurface exhibited exceptional activity and proved that the (111) surface of Pt–Ni had a relatively high activity compared with other surfaces, leading to extensive follow-up studies on the octahedral Pt–Ni nanocrystals [17–20]. However, with buried inactive catalyst atoms and a

---

lack of stability in harsh performance conditions due to the loss of core materials, they offer limited room for development [21,22]. Nanocage (shape-selective and hollow) materials, with unique three-dimensional porous structure, well-defined shape and high surface area-to-volume ratio that allow easy molecular accessibility, are another promising electrocatalyst for ORR [23–25]. Xia et al. has demonstrated that octahedral Pt nanocage showed a factor of 5 enhancement in activity compared to traditional Pt/C [23]. In addition, nanocage materials were proven to show robust stability with no dissolution of unstable core materials [26]. For example, Li et al. found only slightly decreased ORR activity on Pt-enriched icosahedral nanocages after stability testing [25]. In spite of the great progress on Pt based nanocages with different shapes, it is still a great challenge to further enhance the ORR performance.

Herein, we design a novel trimetallic Pt–Pd–Ni octahedral nanocage structure, which are precisely achieved by alloying Ni atoms with octahedral Pt–Pd nanocages. Such octahedral Pt–Pd–Ni nanocages achieve a factor of ~10 enhancement in mass activity (1.17 A/mg$_{Pt}$) and a factor of ~25 enhancement in specific activity (3.8 mA/cm^2) compared to commercial Pt/C due to the synergistic effects of exposed (111) facets, hollow structure and the modulated geometric structure by the incorporation of Ni atoms. In addition, octahedral Pt–Pd–Ni nanocages impressively show only 16% performance fading during ADTs, which significantly outperforms the reported solid octahedral Pt–Ni with similar activity (~60% loss after stability test) [27–29]. To the best of our knowledge, this is the first work to synthesize multimetallic octahedral Pt-based nanocages with high ORR activity and robust stability.

2. Experimental sections

Materials: All the chemicals were used as received from Sigma-Aldrich (unless specified). Sodium tetrachloropalladate (Na$_2$PdCl$_4$, 98%), Potassium tetrachloroplatinate (II) (K$_2$PtCl$_4$, 99.99%), formaldehyde (HCHO), ascorbic acid (AA, 99%), potassium bromide (KBr, 99%), poly (vinyl pyrrolidone) (PVP, MW ≈ 55,000), citric acid (CA, 99.5%), ferric chloride (FeCl$_3$, 97%), hydrochloric acid (HCl, 37%), ethanol (C$_2$H$_6$O), acetic acid (99.7%), nickel nitrate hexahydrate (Ni (NO$_3$)$_2$·6H$_2$O), perchloric acid (HClO$_4$, 70%, PPT Grade), nitric acid (HNO$_3$), commercial Pt/C (wt 40% loading, E-TEK), isopropanol (C$_3$H$_8$O, Sinopharm Chemical Reagent). Nafion solution (5.0 wt %) was purchased from Dupont to prepare the thin film electrode. Deionized water (18.2 MΩ, Mill-Q Corporation) was used for preparing the solutions.

Preparation of Pd cube: 105 mg of PVP, 60 mg of AA, and 300 mg of KBr were dissolved in 8 mL of DI water, which was heated at 80 °C in an oil bath under magnetic stirring for 10 min. Subsequently, 57 mg of Na$_2$PdCl$_4$ was dissolved in 3 mL of DI water and then injected into the pre-heated solution with a pipette. The vial was sealed and maintained at 80 °C for an additional 3 h. The final product was collected by centrifugation, washing for three times with DI water and re-dispersing in 10 mL DI water to form Pd cube suspension.

Preparation of Pd octahedra: 105 mg of PVP, 0.1 mL of HCHO, and 0.3 mL of the as-prepared Pd cube suspension (1.8 mg/mL) were mixed in 8 mL of DI water and then heated at 60 °C for 10 min in an oil bath under magnetic stirring. At the same time, 29 mg of Na$_2$PdCl$_4$ was dissolved in 3 mL of DI water and then injected into the pre-heated solution with a pipette. The reaction mixture was capped and maintained at 60 °C for 3 h. The final product was collected by centrifugation, washed for three times with DI water, and re-dispersed in 2 mL DI water as a Pd octahedra suspension.

Preparation of the nanoscale Pd@Pt octahedra: 70 mg of PVP and 120 mg of CA were added into 23 mL of the prepared Pd octahedra suspension and then heated at 95 °C for 10 min under magnetic stirring. Meanwhile, 5 mg of K$_2$PtCl$_4$ was dissolved in 3 mL of DI water, and the solution was quickly added into the preheated solution using a pipette.

The reaction solution was kept at 95 °C for 24 h under magnetic stirring and then cooled to room temperature. The product was collected by centrifugation, washed three times with DI water, and re-dispersed in DI water as a Pd@Pt octahedra suspension.

Preparation of octahedral Pt$_3$Pd nanocages: 300 mg of KBr, 50 mg of PVP, 30 mg of FeCl$_3$, 0.18 mL of HCl, and 7 mL of DI water were mixed in a glass vial. The mixture was heated to 85 °C in an oil bath under magnetic stirring. Subsequently, 0.2 mL of the as-prepared Pd@Pt octahedra suspension was added using a pipette and stirred for 4 h remove interior Pd atoms. Lastly, the product was collected by centrifugation, washed twice with ethanol and three times with water, and then dispersed in DI water for further use.

Preparation of octahedral Pt$_3$PdNi nanocages: Firstly, Pt$_3$Pd nanocages were loaded on a carbon support. The carbon-supported catalysts were then dispersed in 10 mL of acetic acid and heated at 70 °C for 12 h to clean the surface of the particles, and washed twice with ethanol. 5 mg of Pt$_3$Pd nanocages and 1 mg of Ni (NO)$_3$·6H$_2$O were dispersed ultrasonically in 10 mL deionized water. The homogeneous mixture was immediately frozen by using liquid nitrogen, then dried in a refrigerated drying chamber. The sample was then calcined in 20% H$_2$/Ar atmosphere at 150 °C for 2 h. The sample after pyrolysis is dispersed in 10 mL of 0.1 M HClO$_4$ and stirred overnight at 60 °C. Then the products were collected by centrifugation and washed for four times with deionized water to obtain the final Pt–Pd–Ni octahedral nanocages.

Physical characterization: Transmission electron microscopy (TEM) and high-resolution TEM (HR-TEM) were carried out on FEI Tecnai G2F30 with an acceleration voltage of 300 kV. Scanning transmission electron microscopy (STEM) images and energy dispersive spectroscopy (EDS) were collected on an FEI Titan Cubed Themis G^2 300. The Cu grid was used during all the EDS analyses. X-ray photoelectron spectroscopy (XPS) was performed on a PHI 5700 ECSA System, using Al Kα radiation (1486.6 eV). The composition of catalysts was determined by PerkinElmer Optima 5300DV inductively coupled plasma Optical Emission Spectrometer (ICP-OES). Pt L$_3$ edge- X-ray absorption fine structure (XAFS) spectra were collected on the Hard X-ray Micro-Analysis (HXMA) beamline at the Canadian Light Source (CLS) 06ID-01. X-ray absorption near edge structure (XANES) and extended x-ray absorption fine structure (EXAFS) data reduction was performed using the IFEFFIT based program. Edge step normalization for each spectrum was performed by subtracting the pre-edge and post-edge backgrounds.

Electrochemical testing: The 4 mg catalyst was ultrasonically dispersed in a solution of 3 mL water, 1 mL isopropanol, and 4 μL Nafion (5 wt%) for 10 min (1 mg/mL). The Pt loading of Pt/C, Pt$_3$Pd NCs and Pt$_3$PdNi NCs on rotating disk glassy carbon electrode (5 mm in diameter), which was already polished by 0.3 μm alumina powder in advance, was 20, 4.6 and 4.6 μg cm^{-2}, respectively. Pt foil and reversible hydrogen electrode (RHE) were used as the counter electrode and reference electrode, respectively. Cyclic voltammetry (CV) curves were recorded in an argon saturated 0.1 M HClO$_4$ environment at a scan rate of 100 mV s^{-1}. The electrochemical surface area of Pt (ECSA) is calculated by the integration of the coulombic charges associated with the hydrogen adsorption after correcting for the double - layer charging current:

$$ECSA = \frac{Q_H}{210 \times m_{Pt}}$$

where Q$_H$ (μC) is the charge associated with the hydrogen atom adsorption, 210 (μC cm^{-2}) is the charge related to the monolayer adsorption of the hydrogen atom adsorption on Pt, m$_{Pt}$ is the actual Pt loading on the working electrode.

Oxygen reduction reaction (ORR) polarization curves were recorded in an oxygen saturated 0.1 M HClO$_4$ environment at a scan rate of 10 mV s^{-1} at a rotation rate of 1600 r min^{-1}. All ORR polarization curves are shown after iR correction. The stability test is performed by

applying potential cycles between 0.6 and 1.0 V with a scan rate of 100 mV s^{-1}. All the electrochemical measurements were conducted on an Autolab electrochemical workstation at room temperature.

DFT calculation: Density functional theory (DFT) calculations were performed here with the plane wave-based Vienna *ab initio* simulation package, (VASP) [30]. To better describe the adsorbate adsorption on Pt, the BEEF-vdW functional was used in the combination with the generalized gradient approximation (GGA) [31]. The calculated equilibrium lattice constant of *fcc* Pt is 3.99 Å in good agreement with experimental parameters, 3.92 Å [32]. A 400eV energy cutoff and a force convergence standard of 0.02 eV/Å were qualified to calculate the system. The *k*-point mesh was carefully tested and finally $3 \times 3 \times 1$ was chosen to sample the Brillouin zone for all the calculations. To prevent periodic interactions, a 15 Å spacing was used in the Z direction. The density of states (DOS) of surface Pt was calculated to obtain *d*-centers on different surfaces. The entropies and zero-point energies (ZPE) of surface species were calculated from the vibrational frequencies obtained by DFT using the harmonic oscillator approximation. The adsorption energy of hydroxyl group is calculated as follows.

$$E_{ads/OH} = E_{slab/OH} - E_{slab} - E_{OH} \tag{1}$$

$$G_{ads/OH} = E_{ads/OH} + \Delta ZPE - T\Delta S \tag{2}$$

Where $E_{ads/OH}$ is the DFT adsorption energy of OH, E_{slab} is the energy of clean surface, E_{OH} is the calculated energy of gas-phase hydroxyl, and $G_{slab/OH}$ is the calculated adsorption free energy of different surfaces. ΔZPE is the change in zero-point energy of the adsorbates. T is 298 K here. ΔS is approximated from the loss of entropy of the gas phase molecules upon binding them to the surface.

Models: To simulate different catalytic surfaces in ORR reactions, Pt-based surfaces were all modeled on the same Pt (111) surface: a 5-layer slab of Pt (111) with 3×3 atomic arrangement per layer. For hollow Pt octahedral nanoparticles, the first subsurface of Pt (111) were substituted with 3 Pd atoms and the second subsurface with 2 Pd atoms. For hollow Pt–Ni octahedral nanoparticles, the first and second subsurfaces (second and third layers of the slab) were both doped by 2 Pd and 2 Ni atoms. In this way, a mixed-alloy subsurface with a Pt overlayer were created, consistent with spectroscopic results of these catalysts.

3. Results and discussion

Trimetallic Pt$_3$PdNi octahedral nanocages supported on carbon (Pt$_3$PdNi NCs) were achieved by a multi-step methods, as illustrated in Fig. 1a. Briefly, the as-prepared Pd cubes with an average edge length of 10 nm (shown in Fig. S1) were used as seeds for the formation of well-defined Pd octahedra (shown in Fig. S2). A uniform Pt shell was then deposited onto the surface of Pd octahedra as Pd@Pt. The Pd@Pt presents a well-defined and uniform octahedral morphology (Fig. S3) and a typical core-shell profile where Pd is covered by an ultrathin Pt shell (Figs. S4–S5). The Pt$_3$Pd octahedral nanocages (Pt$_3$Pd NCs) were derived from Pd@Pt octahedra by selectively etching interior Pd atoms. The HAADF-STEM image of Pt$_3$Pd NCs (Fig. S6a) shows a typical octahedral shape and most surfaces are decorated by small holes. The elemental composition is shown to be Pt$_3$Pd by ICP-OES, while Pt and Pd are uniformly distributed across the whole surface, determined by EDS mapping, shown in Figs. S6b–d.

The targeted Pt$_3$PdNi NCs were synthesized by incorporating Ni atoms (derived from Ni(NO$_3$)$_2$·6H$_2$O) into Pt$_3$Pd NCs on carbon through pyrolysis at 150 °C under 20% H$_2$/Ar, followed by acid leaching for 12 h to remove unalloyed Ni atoms. The HAADF-STEM (Fig. 1b) and TEM (Fig. S7a) images of Pt$_3$PdNi NCs suggest a uniform size distribution. Importantly, Pt$_3$PdNi NCs maintain typical nanocage morphology in enlarged HAADF-STEM image (Fig. 1c), where the interior Pd atoms are etched and surfaces are still decorated by small holes. The elemental distribution of Pt$_3$PdNi NCs is revealed through EDS shown in Fig. 1d–i.

The ultrathin shell is composed of Pt, Pd and Ni, indicating Ni atoms are incorporated into the Pt$_3$Pd NCs. In addition, there is almost no elemental signal at the center of Pt$_3$PdNi NCs, further confirming the hollow nature of the nanocage structure. The lattice distance of Pt$_3$PdNi NCs, measured in HR-TEM (Fig. 1j and Figure S7b), is 0.22 nm (shown in Fig. 1k), which is the same as that derived from FFT in Fig. 1j, confirming Pt$_3$PdNi NCs are enclosed by (111) facets. XPS spectra of Pt$_3$PdNi NCs and Pt$_3$Pd NCs in Figure 1l and Fig. S8 show that the majority of Pt on the surface is metallic.

The electrocatalytic ORR performances of Pt$_3$Pd NCs and Pt$_3$PdNi NCs were evaluated using the rotating disk electrode (RDE) method. In addition, commercial Pt/C was also tested as a reference sample. The CV curves of commercial Pt/C, Pt$_3$Pd NCs and Pt$_3$PdNi NCs nanocatalysts were recorded in an argon saturated 0.1 M perchloric acid solution (Fig. 2a). The electrochemically active surface area of Pt$_3$Pd NCs and Pt$_3$PdNi NCs, determined by hydrogen atom underpotential deposition in CV [33], is calculated as 38.6 and 31.8 m^2 g$_{Pt}^{-1}$, respectively, which are comparable with reported cubic, octahedral and icosahedral Pt-enriched nanocage [23,25]. For the purpose of probing the kinetic activity, a representative set of polarization curves for the ORR in oxygen saturated 0.1 M perchloric acid are shown in Fig. 2b. The polarization curves reveal that the ORR kinetics are dramatically accelerated on both Pt$_3$Pd NCs and Pt$_3$PdNi NCs. Comparing with the half-wave potential of commercial Pt/C, significant positive shifts of 43 mV and 30 mV are observed on Pt$_3$PdNi NCs and Pt$_3$Pd NCs, respectively. Tafel plots (Fig. S9) and the slope (Table S1) also confirm the greatly enhanced ORR performance on Pt$_3$PdNi NCs. As shown in Fig. 2c, the specific activity of Pt$_3$PdNi NCs at 0.9 V is ~3.8 mA/cm^2, a factor of 25 enhancement compared to Pt/C and a factor of 2 enhancement over Pt$_3$Pd NCs, respectively. These Pt$_3$PdNi NCs also outperforms single metal nanocages such as cubic, octahedral and icosahedral nanocages and Pt-based multi-metallic hollow nanoparticles (shown in Table S2).

Stability of the nanocatalysts during ADTs is another important indicator for the practical application of PEMFCs. To evaluate the ORR durability of the catalysts, the potential is cycled between 0.6 V and 1.0 V for 10,000 cycles at a sweep rate of 100 mV/s as ADTs. The CV and ECSA of Pt/C, Pt$_3$Pd NCs and Pt$_3$PdNi NCs before and after ADTs are shown in Fig. S10. ECSA of Pt/C shows about 24% decrease, while, a slightly increased ECSA on Pt$_3$PdNi NCs after stability test may be due to the dissolution of inter Ni atoms. The ORR polarization curves and mass activity of Pt NPs, Pt$_3$Pd NCs and Pt$_3$PdNi NCs before and after ADTs are measured as shown in Fig. 3 and Fig. S11. The mass activity of Pt$_3$PdNi NCs is about 0.98 (A mg$_{Pt}^{-1}$), showing a loss of 16% over cycling. The composition of Pt$_3$PdNi NCs is about Pt$_3$PdNi$_{0.8}$, where slight Ni dissolution may account for decay of the performance. However, after durability test, the performance on Pt/C (0.08 A mg$_{Pt}^{-1}$) decreases by 23% compared with their initial activity. A negligible change of morphology of Pt$_3$PdNi NCs in Fig. 3a indicates the robust stability of the structure. Conversely, commercial Pt/C shows Pt nanoparticles aggregation during stress testing (Fig. S12). Notably, Pt$_3$PdNi NCs exhibit a greatly enhanced stability compared to solid Pt–Ni octahedra with similar performance and some recently published Pt based electrocatalysts (shown in Table S3).

In order to understand the superior ORR performance of Pt$_3$PdNi NCs, the X-ray Absorption Spectroscopy (XAS) is used to probe the local atomic structure of the catalyst, which has been reported to impact ORR performance [34,35]. The Pt L$_3$ – edge XANES spectra of the Pt foil, Pt$_3$Pd NCs and Pt$_3$PdNi NCs are shown in Figure 4a, respectively. The threshold energy (E$_0$) of the Pt L$_3$ - edge on Pt$_3$Pd NCs and Pt$_3$PdNi NCs are similar to those of the corresponding Pt foil, confirming their metallic nature. The white line (WL) intensity of Pt L$_3$ (Figure 4a) edges shows the sequence: Pt$_3$Pd NCs < Pt$_3$PdNi NCs. The changes in WL intensity could be caused by ligand effects due to the incorporation of Ni atoms. Quantitative analysis of the EXAFS region of the XAS is used to study the local atomic structure of Pt and the corresponding Fourier transforms is shown in Fig. S13, Fig. 4b and c and Table 1. Pt$_3$PdNi NCs
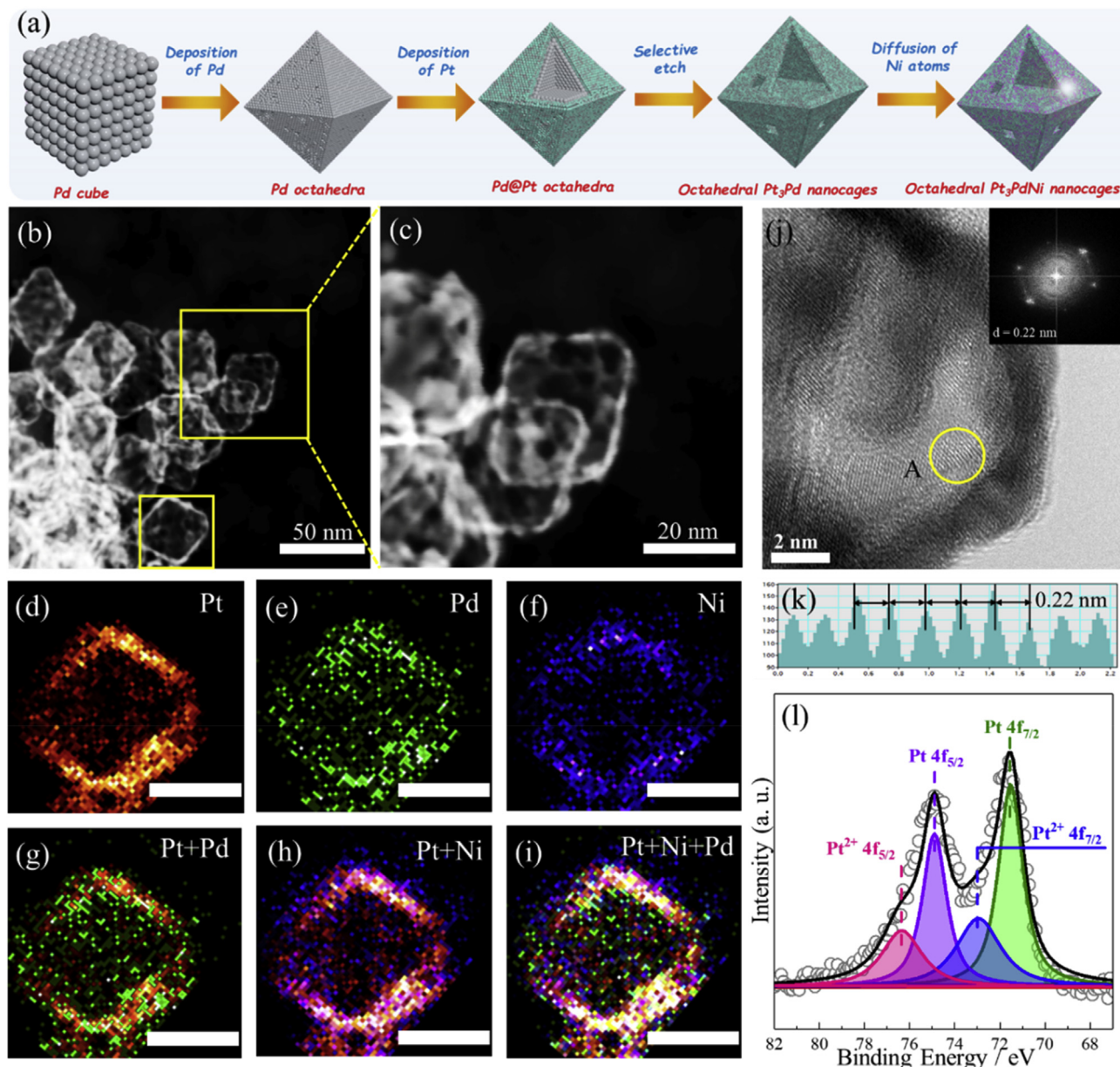
Fig. 1. (a) Schematic diagram of the synthetic route of Pt₃Pd NCs and Pt₃PdNi NCs. (b) HAADF-STEM image of Pt₃PdNi NCs. (c) Enlarged HAADF-STEM image of Pt₃PdNi NCs. EDS element of Pt (d), Pd (e), Ni (f) and mix (g–i), scale bar is 20 nm. (j)The HR-TEM image of Pt₃PdNi NCs. (k) The lattice distance of Pt₃PdNi NCs in area A of Figure j. (l) XPS spectra of Pt₃PdNi NCs.

shows the shortest Pt–Pt bond length (2.72 Å) due to the incorporation of Ni atoms, which correspond to a compressive strain of 0.74% compared to Pt₃Pd NCs. Based on the defined relationship between adsorption energy and Pt–Pt bond length [36], compressive strain can weaken the adsorption energy of OH* on Pt surface and thus improve ORR activity as the OH* desorption is the rate-determining step of ORR on the Pt surface [37].

DFT calculations were also used to further understand improved performance on Pt₃PdNi NCs. Periodic Pt (111), Pt₃Pd (111) and Pt₃PdNi (111) slabs were constructed to represent the surfaces of Pt NPs, Pt₃Pd NCs and Pt₃PdNi NCs, respectively (shown in Fig. S14). After DFT optimization, Pt₃PdNi (111) surface shows 0.8% compressive strain compared to the Pt₃Pd (111) surface (shown in Table S4), consistent with the EXAFS data. The modulated electronic and geometric structure, confirmed by XAS and DFT, are expected to change the DOS of surface Pt atoms and further affect the interaction between the reactant and the surface of catalyst based on previously reported on d-

band theory [38]. The DOS profiles of the three models are shown in Figs. S15–17 and the calculated d-band center are shown in Table S5. The negatively shifted d-band center of Pt₃PdNi (111) referring to the Fermi level could decrease the adsorption energy of the reactant and accelerate the ORR kinetics [38]. On the other hand, The Gibbs energy of the rate determining step intermediate OH* on three models is also calculated to quantitatively understand the increased experimental performance (shown in Fig. 4d-e, and Fig. S18). The Gibbs energy of OH* on Pt₃PdNi (111) is 0.13 eV weaker than that on Pt₃Pd (111), indicating the introduction of Ni could weaken the adsorption energy of OH* and improve ORR kinetics as suggested.

Single metal nanocages and Pt-based hollow structures have been reported to show improved stability repeatedly [25,26,39]. Here, tri-metallic Pt₃PdNi octahedral nanocages also exhibit enhanced stability. It has been revealed that the dissolution of Pt atoms during ADT tests mainly accounts for the deactivation of Pt based catalysts [40]. On the other hand, it has been found that the rate of Pt dissolution increases
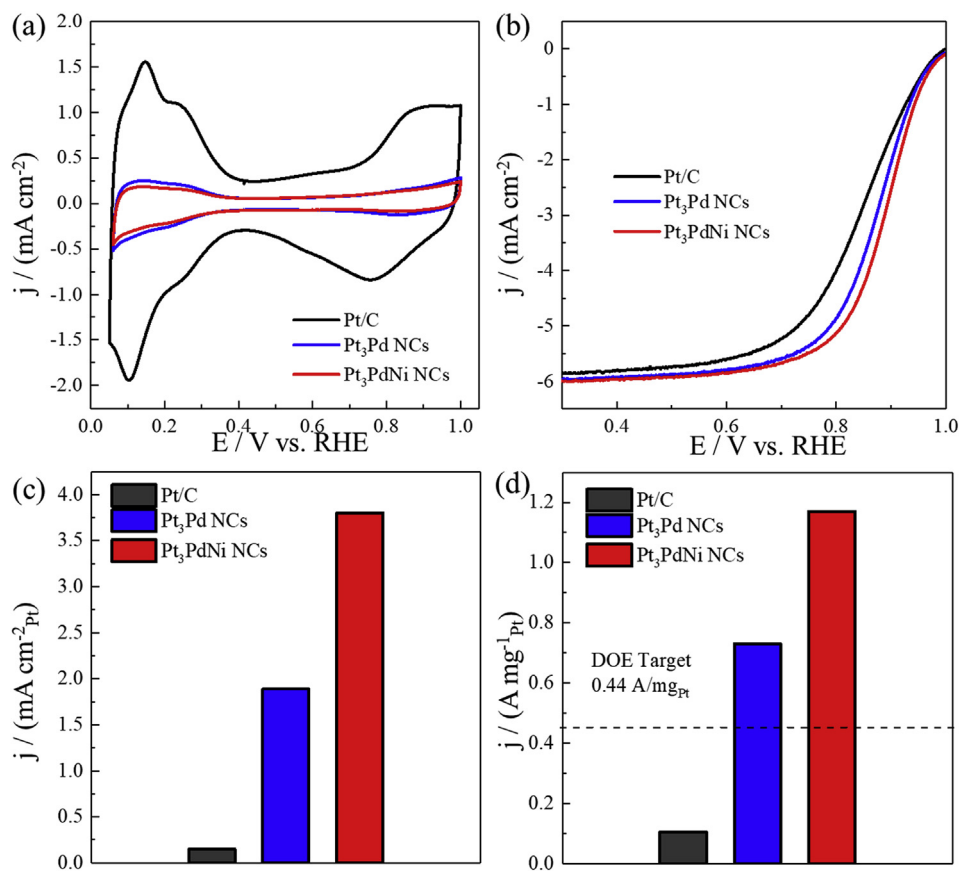
Fig. 2. (a) CV of Pt/C, Pt$_3$PdNi NCs and Pt$_3$PdNi NCs in Ar saturated 0.1 M HClO$_4$. (b) Polarization curves of Pt/C, Pt$_3$PdNi NCs and Pt$_3$PdNi NCs in O$_2$ saturated 0.1 M HClO$_4$ at a rotation rate of 1600 r min^{-1} (scan rate = 10 mV s^{-1}). (c) Specific activities and (d) mass activities at 0.9 V of Pt/C, Pt$_3$PdNi NCs and Pt$_3$PdNi NCs.

sharply with the declining size [40]. For Pt$_3$PdNi NCs, larger 3-D structure and interior Pd both are helpful for the stabilization compared to solid Pt NPs due to the decreased surface energy and preferential Pd oxidation, which both protect surface Pt atoms from oxidation and dissolution [41–43]. DFT calculations are also used to further understand robust stability of Pt$_3$PdNi NCs. The vacancy formation energy of surface Pt atoms can be considered as a rational parameter to reflect the tendency of dissolution of surface Pt atoms and the stability of Pt-based catalysts [44]. The vacancy formation energy of Pt atoms on three models as shown in Figure 4d, f and Fig. S19 – S20, are powerful to reveal the increased stability of Pt$_3$PdNi NCs. As exhibited in Figure 4f,

Pt$_3$PdNi (111) shows the highest vacancy formation energy (E_{VPt} = −0.97eV) compared to Pt (111) (E_{VPt} = −1.14eV) and Pt$_3$Pd (111) (E_{VPt} = −1.12eV), confirming the excellent stability of Pt$_3$PdNi NCs again.

4. Conclusion

Trimetallic octahedral Pt$_3$PdNi NCs with ultrathin wall were successfully synthesized, confirmed by HAADF-STEM-EDS. Compared to Pt$_3$Pd NCs, octahedral Pt$_3$PdNi NCs nanocatalysts show a modulated electronic and geometric structure because of the incorporation of Ni
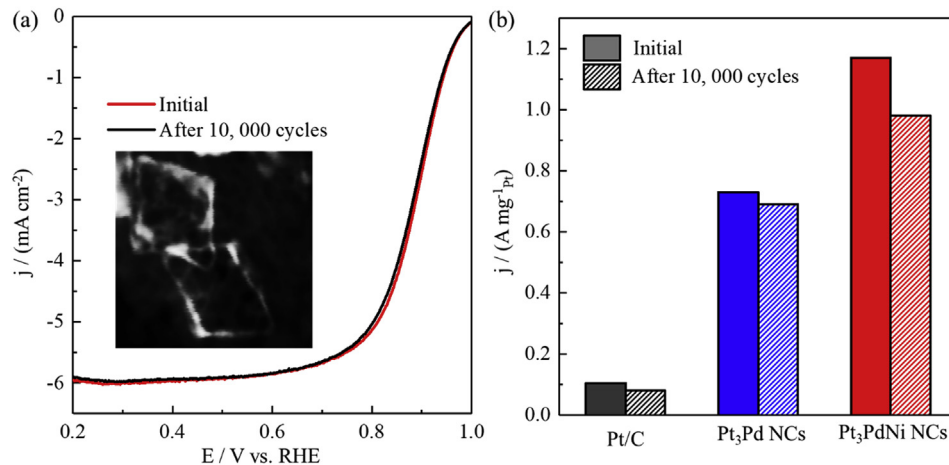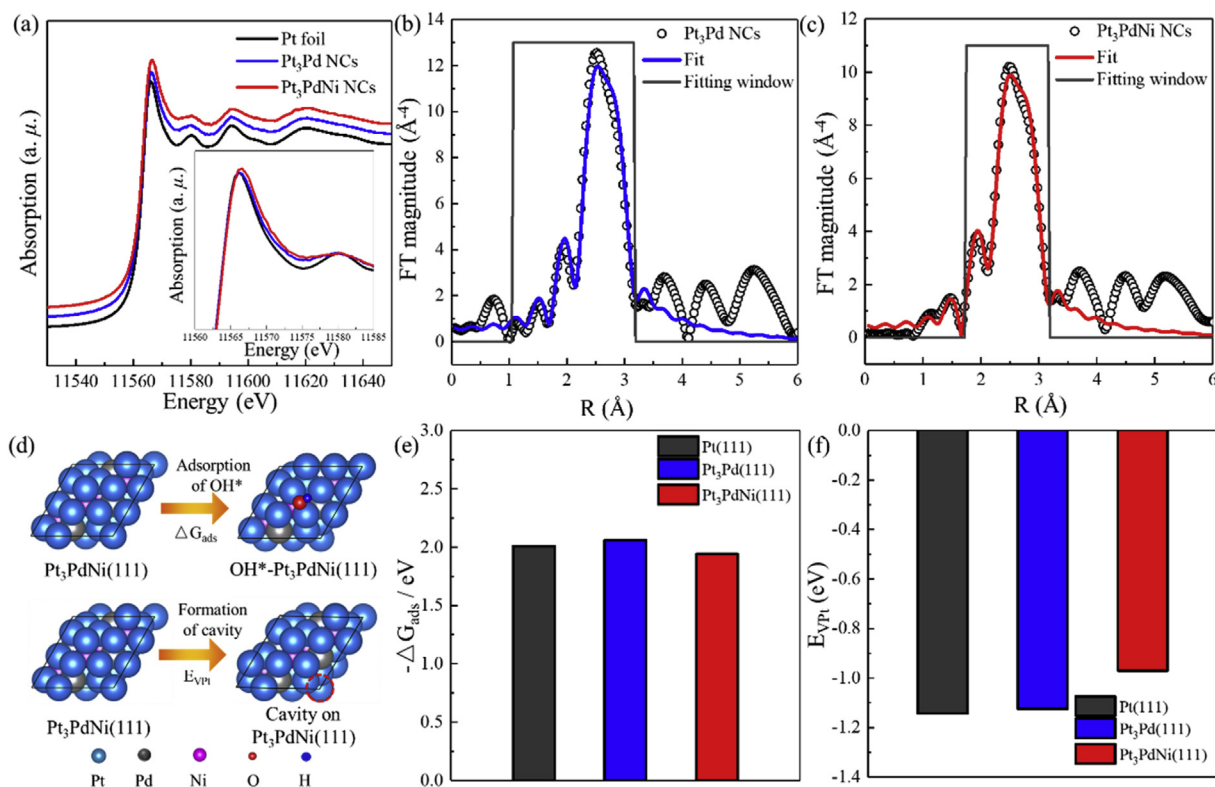

Fig. 3. Polarization curves of Pt$_3$PdNi NCs in oxygen saturated 0.1 HClO$_4$ before and after 10,000 potential cycles between 0.6 and 1.0 V versus RHE. The insert image is the HAADF-STEM image of Pt$_3$PdNi NCs after ADT. (b) mass activities at 0.9 V of Pt/C, Pt$_3$Pd NCs and Pt$_3$PdNi NCs before and after ADT test.

Fig. 4. (a) Normalized XANES spectra of Pt$_3$Pd NCs and Pt$_3$PdNi NCs at Pt L$_3$ edge. EXAFS spectra of Pt$_3$Pd NCs (b) and Pt$_3$PdNi NCs (c) at Pt L$_3$ edge. (d) The theoretical models of adsorption of OH* on the surface of Pt$_3$PdNi (111) and formation of Pt atom vacancy at surface of Pt$_3$PdNi (111). (e) The Gibbs energy of OH* on Pt (111), Pt$_3$Pd (111) and Pt$_3$PdNi (111) slabs. (f) The vacancy formation energy for Pt (111), Pt$_3$Pd (111) and Pt$_3$PdNi (111).

Table 1
Pt L$_3$ edge EXAFS fitting results.

Sample	E$_0$	shell	CN	R(Å)	ΔE$_0$	$\sigma^2(10^{-3}$Å$^2)$	R factor
Pt foil	11564.0	Pt–Pt	12	2.76	8.7	4.9	0.001
Pt$_3$Pd NCs	11564.0	Pt–O	0.23	1.95	7.11	5.0	0.009
		Pt–Pt	10.96	2.74			
Pt$_3$PdNi NCs	11564.1	Pt–O	0.39	2.02	5.42	6.0	0.002
		Pt–Pt	10.88	2.72			

atoms, verified by the EXAFS. DFT calculations, was also used to deeply understand the outstanding performance, revealed a negative shift of the *d*-band center and a weaker adsorption of OH* on Pt$_3$PdNi surface. On the other hand, Trimetallic octahedral Pt$_3$PdNi NCs also show a robust stability compared to that of the commercial Pt. We believe that octahedral Pt$_3$PdNi NCs is a new class of catalyst for ORR.

Appendix A. Supplementary data

Supplementary data to this article can be found online at https://doi.org/10.1016/j.nanoen.2019.103890.

References

[1] I. Staffell, D. Scamman, A. Velazquez Abad, P. Balcombe, P.E. Dodds, P. Ekins, N. Shah, K.R. Ward, Energy Environ. Sci. 12 (2019) 463.
[2] J. Greeley, N.M. Markovic, Energy Environ. Sci. 5 (2012) 9246.
[3] Y. Shao, Y. Cheng, W. Duan, W. Wang, Y. Lin, Y. Wang, J. Liu, ACS Catal. 5 (2015) 7288.
[4] I. Katsounaros, S. Cherevko, A.R. Zeradjanin, K.J. Mayrhofer, Angew. Chem. Int. Ed. 53 (2014) 102.
[5] N. Tian, B. Lu, X. Yang, R. Huang, Y. Jiang, Z. Zhou, S. Sun, Electrochem. Energy Rev. 1 (2018) 54.
[6] B. Han, C.E. Carlton, A. Kongkanand, R.S. Kukreja, B.R. Theobald, L. Gan, R. O'Malley, P. Strasser, F.T. Wagner, Y. Shao-Horn, Energy Environ. Sci. 8 (2015) 258.
[7] R. Wang, H. Wang, F. Luo, S. Liao, Electrochem. Energy Rev. 1 (2018) 324.
[8] J. Luo, L. Wang, D. Mott, P.N. Njoki, Y. Lin, T. He, Z. Xu, B.N. Wanjana, I.I.S. Lim, C.-J. Zhong, Adv. Mater. 20 (2008) 4342.
[9] G. Chen, K. Kuttiyiel, D. Su, M. Li, C. Wang, D. Buceta, C. Du, Y. Gao, G. Yin, K. Sasaki, M. Vukmirovic, R. Adzic, Chem. Mater. 28 (2016) 5274.
[10] M. Nesselberger, M. Roefzaad, R.F. Hamou, P.U. Biedermann, F.F. Schweinberger, S. Kunz, K. Schloegl, G.K. Wiberg, S. Ashton, U. Heiz, K.J. Mayrhofer, M. Arenz, Nat. Mater. 12 (2013) 919.
[11] G. Chen, K.A. Kuttiyiel, M. Li, D. Su, L. Du, C. Du, Y. Gao, W. Fei, G. Yin, K. Sasaki, R.R. Adzic, J. Mater. Chem. 6 (2018) 20725.
[12] L. Gan, M. Heggen, S. Rudi, P. Strasser, Nano Lett. 12 (2012) 5423.
[13] C. Wang, M. Chi, D. Li, D. Strmcnik, D. van der Vliet, G. Wang, V. Komanicky, K.-C. Chang, A.P. Paulikas, D. Tripkovic, J. Pearson, K.L. More, N.M. Markovic, V.R. Stamenkovic, J. Am. Chem. Soc. 133 (2011) 14396.
[14] J. Li, Z. Xi, Y.T. Pan, J.S. Spendelow, P.N. Duchesne, D. Su, Q. Li, C. Yu, Z. Yin, B. Shen, Y.S. Kim, P. Zhang, S. Sun, J. Am. Chem. Soc. 140 (2018) 2926.
[15] K.A. Kuttiyiel, K. Sasaki, Y. Choi, D. Su, P. Liu, R.R. Adzic, Energy Environ. Sci. 5 (2012) 5297.
[16] C. Koenigsmann, A.C. Santulli, K. Gong, M.B. Vukmirovic, W.P. Zhou, E. Sutter, S.S. Wong, R.R. Adzic, J. Am. Chem. Soc. 133 (2011) 9783.
[17] V.R. Stamenkovic, B. Fowler, B.S. Mun, G. Wang, P.N. Ross, C.A. Lucas, N.M. Markovic, Science 315 (2007) 493.
[18] J. Zhang, H.Z. Yang, J.Y. Fang, S.Z. Zou, Nano Lett. 10 (2010) 638.
[19] C. Zhang, S.Y. Hwang, A. Trout, Z. Peng, J. Am. Chem. Soc. 136 (2014) 7805.
[20] C. Cui, L. Gan, M. Heggen, S. Rudi, P. Strasser, Nat. Mater. 12 (2013) 765.
[21] Y. Kang, J. Snyder, M. Chi, D. Li, K.L. More, N.M. Markovic, V.R. Stamenkovic, Nano Lett. 14 (2014) 6361.
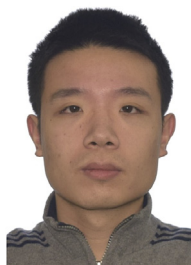[22] K. Sasaki, H. Naohara, Y. Cai, Y.M. Choi, P. Liu, M.B. Vukmirovic, J.X. Wang,

R.R. Adzic, Angew. Chem. Int. Ed. 49 (2010) 8602.
[23] L. Zhang, L.T. Roling, X. Wang, M. Vara, M. Chi, J. Liu, S.I. Choi, J. Park, J.A. Herron, Z. Xie, M. Mavrikakis, Y. Xia, Science 349 (2015) 412.
[24] X. Wang, L. Figueroa-Cosme, X. Yang, M. Luo, J. Liu, Z. Xie, Y. Xia, Nano Lett. 16 (2016) 1467.
[25] D.S. He, D. He, J. Wang, Y. Lin, P. Yin, X. Hong, Y. Wu, Y. Li, J. Am. Chem. Soc. 138 (2016) 1494.
[26] J.X. Wang, C. Ma, Y. Choi, D. Su, Y. Zhu, P. Liu, R. Si, M.B. Vukmirovic, Y. Zhang, R.R. Adzic, J. Am. Chem. Soc. 133 (2011) 13551.
[27] L.G. Chunhua Cui, Marc heggen, stefan Rudi and Peter strasser, Nat. Mater. 12 (2013).
[28] V. Beermann, M. Gocyla, E. Willinger, S. Rudi, M. Heggen, R.E. Dunin-Borkowski, M.G. Willinger, P. Strasser, Nano Lett. 16 (2016) 1719.
[29] R.M. Aran-Ais, F. Dionigi, T. Merzdorf, M. Gocyla, M. Heggen, R.E. Dunin-Borkowski, M. Gliech, J. Solla-Gullon, E. Herrero, J.M. Feliu, P. Strasser, Nano Lett. 15 (2015) 7473.
[30] G. Kresse, J. Furthmüller, Phys. Rev. B: Condens. Mater.Chem. Phys. 54 (1996) 11169.
[31] J. Wellendorff, K.T. Lundgaard, A. Møgelhøj, V. Petzold, D.D. Landis, J.K. Nørskov, T. Bligaard, K.W. Jacobsen, Phys. Rev. B: Condens. Mater.Chem. Phys. 85 (2012) 235149.
[32] W.M. Haynes, CRC Handbook of Chemistry and Physics, 94th ed., Taylor and Francis, Boca Raton, 2014.
[33] V. Stamenkovic, T.J. Schmidt, P.N. Ross, N.M. Markovic, J. Phys. Chem. B 106 (2002) 11970.
[34] N. Becknell, Y. Kang, C. Chen, J. Resasco, N. Kornienko, J. Guo, N.M. Markovic, G.A. Somorjai, V.R. Stamenkovic, P. Yang, J. Am. Chem. Soc. 137 (2015) 15817.
[35] J. Zhang, M.B. Vukmirovic, Y. Xu, M. Mavrikakis, R.R. Adzic, Angew. Chem. Int. Ed. 117 (2005) 2170.
[36] M. Escudero-Escribano, P. Malacrida, M.H. Hansen, U.G. Vej-Hansen, A. Velazquez-Palenzuela, V. Tripkovic, J. Schiotz, J. Rossmeisl, I.E. Stephens, I. Chorkendorff, Science 352 (2016) 2073.
[37] J.X. Wang, N.M. Markovic, R.R. Adzic, J. Phys. Chem. B 108 (2004) 4127.
[38] V.R. Stamenkovic, B.S. Mun, K.J.J. Mayrhofer, P.N. Ross, N.M. Markovic, J. Am. Chem. Soc. 128 (2006) 8813.
[39] L. Dubau, T. Asset, R. Chattot, C. Bonnaud, V. Vanpeene, J. Nelayah, F. Maillard, ACS Catal. 5 (2015) 5333.
[40] S.G. Rinaldo, J. Stumper, M. Eikerling, J. Phys. Chem. C 114 (2010) 5773.
[41] R. Wang, C. Xu, X. Bi, Y. Ding, Energy Environ. Sci. 5 (2012) 5281.
[42] R. Wang, D. Higgins, S. Prabhudev, D. Lee, J. Choi, M. Hoque, G. Botton, Z. Chen, J. Mater. Chem. 3 (2015) 12663.
[43] K. Sasaki, N. Marinkovic, H. Isaacs, R.R. Adzic, ACS Catal. 6 (2016) 69.
[44] H. Huang, K. Li, Z. Chen, L. Luo, Y. Gu, D. Zhang, C. Ma, R. Si, J. Yang, Z. Peng and J. Zeng, J. Am. Chem. Soc. (139)2017 8152.

Junjie Li is currently a Ph.D. candidate in Prof. Xueliang (Andy) Sun's Group at the University of Western Ontario, Canada. He received his M.S. degree in physical chemistry from University of Science and Technology of China in 2017. Currently, he is working on the synthesis of advanced nanomaterials for fuel cell applications.

Dr. Lei Du received his PhD degree at the year of 2017 from Harbin Institute of Technology, China. He is currently a lecturer at Harbin Institute of Technology. His main research interests include electrocatalysis, mechanism and devices in renewable energy conversion and storage.

Dr. Mohammad Norouzi Banis is a research engineer in Prof. Xueliang (Andy) Sun's group at the University of Western Ontario, Canada. He received his Ph.D. degree in 2013 in Materials Science and Engineering from Western University, on the study of nanostructured low temperature fuel cells and application of x-ray absorption spectroscopy in energy related systems. His current research interests include study of metal ion, metal air and nanocatalysts via in-situ synchrotron-based techniques.

Dr. Lei Zhang received his BS degree in Chemistry (2008) and PhD degree in Nanomaterial Chemistry (2014) from Xiamen University with Prof. Zhaoxiong Xie. He was a visiting graduate student at Georgia Institute of Technology in Prof. Younan Xia's group from 2012 to 2014. From 2015 to 2016, he worked as a Postdoc at Collaborative Innovation Center of Chemical Science and Engineering in Tianjin University. He is currently a postdoctoral associate with Prof. Xueliang Sun at Western University. His research interests include the design and synthesis of metal nanomaterials and single atom catalysts for fuel cells and water splitting devices.

Fanpeng Kong is currently a Ph.D. candidate under the supervision of Prof. Geping Yin in Harbin Institute of Technology (HIT), China. At the same time, he is a visiting student at Prof. Xueliang (Andy) Sun's Advanced Materials for Clean Energy Group, Western University, Canada. His current research interest focuses on the design and preparation of single atom and nanomaterials for oxygen reduction, hydrogen evolution and small organic molecule oxidation.

Sihang Liu studied chemical engineering and received his BS degree from Tianjin University in 2017 and is pursuing his MS degree also in Tianjin University under the guidance of Prof. Jinlong Gong and Prof. Zhi-Jian Zhao. His major research interests include computational catalysis and theoretical chemistry via density functional theory (DFT) and other *ab initio* methodologies. His research topic now is to rationalize computational models under actual reaction conditions.

Guangyu Chen is currently working as a post-doctoral research associate at Harbin Institute of Technology (HIT). He received his Ph.D. in Chemical Engineering and Technology from HIT in 2017. His research interests focus on the polymer electrolyte membrane fuel cells and electrocatalysis.

Kieran Doyle-Davis received his Honours BSc in Physics from McMaster University in 2018, with research focus on process optimization for lithium ion battery fabrication, and thin polymer films. Kieran is currently an MESc candidate at the University of Western Ontario under the supervision of Prof. Xueliang Sun. His current research interests include the development of next generation surface modified 3-D current collectors for both solution and solid-state lithium ion batteries.

Dr. Chunyu Du is a Professor at the School of Chemistry and Chemical Engineering at Harbin Institute of Technology, China. He has engaged in research in the field of Li ion batteries and fuel cells for more than ten years and has published about 130 research papers in refereed journals. His main research interests include the development of fuel cells, novel electrode materials for high energy density batteries and the degradation mechanisms of lithium ion batteries.
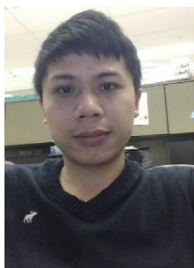
Jianneng Liang is currently a Ph.D. candidate in the department of Mechanical and Materials Engineering at the University of Western Ontario, Canada. He got his B.S. in metallurgical engineering in 2015 from Central South University, China. Currently, his research interests include solid-state polymer electrolytes, hybrid electrolyte, all-solid-state LIBs and Li–S batteries, and the interfacial study in all-solid-state batteries.
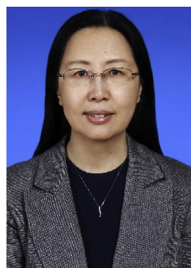
Dr. Geping Yin is a professor at the Harbin Institute of Technology. She received her PhD degree in the year 2000 at the Harbin Institute of Technology supervised by Prof. Derui Zhou. Prof. Yin worked at the Tokyo Institute of Technology (1985) and Yokohama National University (2008) as a visiting scholar. She focuses on the fields of advanced electrode materials, chemical power source systems, etc.
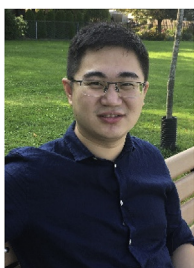
Sizhe Wang is currently a Ph.D. candidate at School of materials and energy, University of Electronic Science and Technology of China (UESTC), China. At the same time, he is a visiting student in Prof. Xueliang (Andy) Sun's Nanomaterials and Energy Group at University of Western Ontario, Canada. He got his B.S. degree in Electronics Science and Technology from School of Microelectronics and Solid-State Electronics, UESTC, in 2013. Currently, his research interests focus on nanocarbon and advanced functional materials as well as their applications in energy conversion and storage, especially for Na/Li-ion batteries and Li–S batteries.
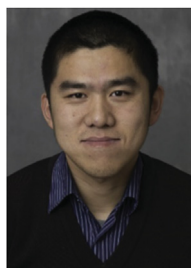
Zhi-Jian Zhao received his BS and MS degrees in chemistry from Zhejiang University (supervisor Prof. Qi Wang) in 2008 and his PhD degree from Technische Universität München (supervisor Prof. N. Rösch) in 2012. After working as Postdoc with Prof. J. Greeley in Purdue University and Dr F. Studt, Prof. J. Nørskov in Stanford University, he joined the faculty of Tianjin University in 2015 as an Associate Professor. He also serves as associate editor for Chemical Engineering Science. His current research interest lies in molecular mechanistic understanding of heterogeneous catalytic reactions.

Feipeng Zhao is currently a Ph.D. candidate in Prof. Xueliang (Andy) Sun's Group at the University of Western Ontario, Canada. He received his B.S. degree and M.S. degree in Materials Science from Soochow University in 2017 and 2014, respectively. Currently, he is working on the synthesis and characterization of sulfide electrolytes, and development of high-performance solid-state Li metal and Na metal batteries.

Prof. Xueliang (Andy) Sun is a Canada Research Chair in Development of Nanomaterials for Clean Energy, Fellow of the Royal Society of Canada and Canadian Academy of Engineering and Full Professor at the University of Western Ontario, Canada. Dr. Sun received his Ph.D. in materials chemistry in 1999 from the University of Manchester, UK, which he followed up by working as a postdoctoral fellow at the University of British Columbia, Canada and as a Research Associate at L'Institut National de la Recherche Scientifique (INRS), Canada. His current research interests are focused on advanced materials for electrochemical energy storage and conversion, including electrocatalysis in fuel cells and electrodes in lithium-ion batteries and metal-air batteries.

Ruying Li is a research engineer at Prof. Xueliang (Andy) Sun's Nanomaterial and Energy Group at the University of Western Ontario, Canada. She received her master in Material Chemistry under the direction of Prof. George Thompson in 1999 at University of Manchester, UK, followed by work as a research assistant under the direction of Prof. Keith Mitchell at the University of British Columbia and under the direction of Prof. Jean-Pol Dodelet at l'Institut national de la recherché Scientifique (INRS), Canada. Her current research interests are associated with synthesis and characterization of nanomaterials for electrochemical energy storage and conversion.